Ambient Diagnostics

Yang Cai[1], Gregory Li[1], Teri Mick[1], Sai Ho Chung[1], and Binh Pham[2]

[1] Carnegie Mellon University, USA
{ycai,gregli,teri}@cmu.edu, saic@andrew.cmu.edu
[2] Queensland University of Technology, Australia
b.pham@qut.edu.au

1 Introduction

People can usually sense troubles in a car from noises, vibrations, or smells. An experienced driver can even tell where the problem is. We call this kind of skill *'Ambient Diagnostics'*.

Ambient Diagnostics is an emerging field that is aimed at detecting abnormities from seemly disconnected ambient data that we take for granted. For example, the human body is a rich ambient data source: temperature, pulses, gestures, sound, forces, moisture, et al. Also, many electronic devices provide pervasive ambient data streams, such as mobile phones, surveillance cameras, satellite images, personal data assistants, wireless networks and so on.

The *peripheral vision* of the redundant information enables Ambient Diagnostics. For example, a mobile phone can also be a diagnostic tool. As the sounds generated by breathing in asthma patients are widely accepted as an indicator of disease activity [1, 2], researchers have investigated the use of a mobile phone and electronic signal transfer by e-mail and voice mail to study tracheal breath sounds in individuals with normal lung function and patients with asthma [3]. The results suggest that mobile phone recordings clearly discriminate tracheal breath sounds in asthma patients and could be a non-invasive method of monitoring airway diseases.

It is challenging to extract just one bit of diagnosis (positive or negative) from massive ambient data. First, we need pivotal heuristics or domain knowledge. In many cases, the heuristics just serve as an early warning rather than an accurate examination. For example, medical studies show that snoring may be related to hypertension, cardiac dysfunction, angina pectoris and cerebral infarction. The immediate rise in systemic blood pressure during snoring has been confirmed by polygraphic recordings [60]. A 'snoremeter' could be added into a mobile phone because it already has a microphone inside. It would provide valuable early warnings for related diseases.

Second, we need *physical heuristics* that effectively filter out the trivial data while only keeping the abnormities. Knowing the physical properties of the targeted system would greatly benefit a diagnosis. For example, if we know that the needle in a hay stack is metal, then we can work around the metal properties and make the hay disappear. Ideally, physical heuristics map the data to a feature space that only displays limited interesting features. Determining which

Y. Cai (Ed.): Ambient Intelligence for Scientific Discovery, LNAI 3345, pp. 224–247, 2005.

modality to use for mapping the feature space is sometimes called *'modality intelligence.'* For instance, classic Fourier Transformation algorithms map data from a time-domain to a frequency-domain. For many periodical data sets, this is a blessing because it is easier to see the patterns in the frequency domain. Wu and Siegel developed a sound recognition system that can identify types of vehicles by sound signatures [11]. The algorithm can also be used for analyzing the breathing patterns of asthma sufferers.

Third, we need effective feature descriptions. The human brain is mainly wired using languages, not for pixel computations. How to transform a verbal description into a digital representation is a non-trivial task. For example, how do we describe the texture on the human body? How do we sense group activities in a video from a nursing home?

Ambient Diagnostics can be traced back to ancient times. For over two thousand years, physical inspection has been a unique and important diagnostic method of Traditional Chinese Medicine (TCM). Observing abnormal changes in the tongue, blood volume pulse patterns, breath smells, gestures, etc., can aid in diagnosing diseases. TCM diagnosis is a black-box approach that involves only input and output data around the body. For many years, scientists have been trying to use modern technologies to unleash the ancient knowledge base. For example, a recent paper published on an IEEE conference presents a computer-based arterial blood-volume pulse analyzer. It is a 'rediscovery' of the diagnostic method originated from ancient TCM [65].

This chapter was inspired by the research of computerized TCM tongue inspection. Through this case study, the chapter discusses the components and potential of ambient diagnostics. We believe that it can be used in applications such as security intelligence, where the difference is deceiving.

2 Tongue Inspection

Visual inspection of the tongue has been a unique and important diagnostic method of Traditional Chinese Medicine (TCM) for thousands of years. Observing the abnormal changes in the tongue proper and in the tongue coating can aid in diagnosing diseases. The inspection of the tongue comprises the inspection of the tongue body and the coating. The tongue body refers to the tissue of the muscle and blood vessels, while the coating refers to something on the tongue like mosses, which are formed, according to the theory of TCM, by the rising of the 'qi' (energy) of the spleen and stomach. For decades, international TCM medical professionals have conducted an enormous number of scientific experiments on tongue inspection [26].

Clinical data has shown significant connections between various viscera cancers and abnormalities in the tongue and the tongue coating. Yao from China studied 4,000 clinical cases with gastroendoscopy images over a period of 20 years. He found significant connections between various viscera cancers and abnormalities in the tongue and the tongue coating. Yao found that viscera cancer patients showed less tongue coating at the tip or edge of the tongue and that

the coating color had turned to purple. He published a book about his study, including in it 130 tongue inspection images, along with gastroendoscopy images and patient diagnoses [20].

Since the early 1980s, medical professionals in China have systematically studied the relationship between various cancers and tongue signatures. Their results have been published in national medical journals. For instance, China TCM Society, China Cancer Society and TCM Diagnosis Association conducted a national project that included cases of 12,448 cancerous patients, 1,628 non-cancerous patients and 5,578 normal patients. The results statistically showed that there are significant changes of color, coating, shape and dorsum shape of the tongues of cancerous patients versus those tongues of non-cancerous patients or normal subjects [23]. Fujin TCM Hospital in China conducted a survey of 168 stomach cancer patients and 200 healthy subjects in 1983. The results showed that the percentage of abnormal tongues were 4 to 10 times higher in cancerous patients than those of healthy subjects; for example, for cancer patients: 70.8% purple/bluish color, 76.5% abnormal proper coating, 20.8% with cracks, and 83.9% dorsum deformation, and for healthy subjects: only 12.5% purple/bluish color, 26.2% abnormal proper coating, 1.5% with cracks, and 10.5% with dorsum deformation [25]. PLA 211 Hospital in China conducted a series of surveys on liver cancer patients versus non-cancer patients who have liver diseases. Results showed that liver cancer patients' abnormal tongue percentage is about 2 to 3 times higher than those of non-cancerous patients [21]. The data shows the method has certain selectivity for cancer diagnosis. Another survey showed that the level of abnormal signatures on the tongue increased as the tumor size increased from less than 5mm, larger than 5mm, to wide spread. The data shows promise for cancer stage estimation and possible early diagnosis [63].

Visual inspection of the tongue offers many advantages: it is a non-invasive diagnosis method, is simple and inexpensive. However, the current practice in TCM is mainly experience based or subjective. The quality of the visual inspection varies between individuals. Although there are a few experts successfully diagnosing cancers based on inspection of the tongue, their skills are not easily transferable to other medical professionals. Their expertise is limited to qualitative descriptions, not to quantitative or mathematical formulations. To circumvent this problem, studies have investigated and reported options such as fuzzy logic [30] and image analysis [31]. Here we discuss a computerized vision system for tongue inspection.

In this study, we investigate a novel imaging system for visual inspection of the tongue [19]. The objectives are to use a digital camera to make an image of a patient's tongue, then use software to extract the features from the digital image created, and finally make a diagnosis based on quantitative models. *The goal is not to replace the conventional diagnostic methods but to give an early alert signal* that can lead to further diagnosis by other methods, such as MRI, CT, X-ray, etc. This novel approach has various significant advantages. First, it makes the inspection objective and repeatable so that it prevents human bias and errors. Second, it can be implemented on an inexpensive personal computer

or laptop computer for clinic or family use. Third, it's a unique exploration to combine Traditional Chinese Medicine (TCM) with contemporary computer vision technologies. The results of this project may inspire future long-term development of bio-computing technologies and further the use of computers in the medical field.

Studies show that there are correlations between the digestic diseases and tongue feature changes. Here we focus on colon polyps that would likely become colon cancer. This pilot study phase focuses on a preliminary investigation of the computer-based tongue inspection technology. A set of computer vision models have been developed to simulate the TCM diagnosis, for example, images that showed detectable cancer signatures such as color and coating texture of the tongue. Those visual feature descriptions will eventually be integrated into a decision-making model that will help to generate the final diagnosis or conclusion: normal, abnormal, likelihood of cancer, etc. The software includes the following issues: 1) *Segmentation:* The raw images are preprocessed with color normalized so that they have better numerical representation. Then each image is segmented to remove the background. The Deformable Template algorithm is applied to generate an accurate outline of the tongue. After the initial image processing, the improvement of the color normalization and segmentation is investigated. 2) *Texture feature extraction:* The texture, which includes cracks and distributions of the tongue proper, is the most important feature. It is the most challenging task in the project because the texture is not uniformly distributed and the orientation and size varies from image to image. 3) *Visualization models:* With the color measurement and texture features, a set of visualization methods are explored. 4) *Diagnosis with Neural Computing:* Artificial neural networks are used to classify samples.

3 Tongue Imaging

We have explored two scientific methods for tongue imaging so that we can recover the realistic measurement of physical values. The first approach is to use a modified hand-held color scanner with a microscopy slide on top of the tongue. As the scanner is gently moved from the root of the tongue to the tip, a flat image can be obtained. Figure 1 shows a sample image. The advantage of this method is its simplicity; it can avoid major color calibration and the removal of artifacts. However, it is a contact measurement that we want to try to avoid in a clinical environment, and the hardware needs to be specially designed to fit the size of tongues. The second approach is to take a picture of the tongue with a commercial digital camera (640 x 480 pixels) plus a Munsell ColorChecker [27] embedded inside the image. Since we already know the color value of the test cells on ColorChecker, we can calibrate the color of the image computationally.

Because the color in an image varies with cameras, lighting and equipment settings, we had to calibrate the color for each image before the analysis. We used the Mansall color calibration board and the newly developed color calibration software. Before the camera took a tongue image, the operator took a

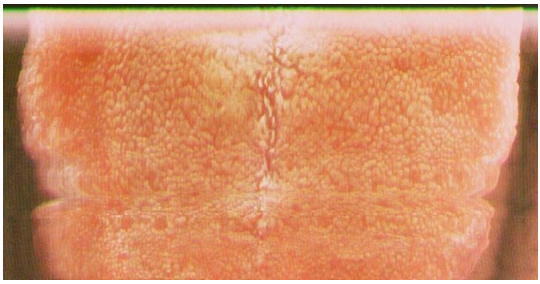

Fig. 1. First image from the tongue scanner.

picture of the calibration board and saved it along with the tongue image. Then the computer performed the color calibration for the data. At this phase, we developed and tested the color calibration software.

A semi-automatic color calibration tool was developed for the project. By manually clicking the four corners of the ColorChecker, the software can perform the transformation and find the points in each square. Then a linear color calibration model is used to recover the original color of the tongue under various lighting conditions [27].

Parallel to the data collection from cancerous patients, tongue images were also collected from healthy subjects for studying the range of the deviation and mean of the 'normal' tongue images, such as RGB color space, coating texture, etc. Over 17 'normal' tongue images were collected in the database. Those images helped to establish a baseline for a 'normal tongue.'

We tested 17 tongue images taken from a "healthy" individual with a digital camera under different combinations of illumination and lighting orientations. The illumination conditions were daylight and indoor lighting in an office. 160 points from each tongue image were sampled to generate the data as shown in Table 1.

4 Segmentation of Tongue Image

There are many ways to segment the tongue area from the background. Color-based segmentation is the least reliable way because of the variations of tongue color and shadows. Active Contour may overcome the color variation problems by tracking the gradient of the intensity along the tongue edge. The typical al-

Table 1. Color variations of a normal tongue under different conditions.

Color	*Before Calibrated*		*After Calibrated*	
Space	**Mean**	**STD**	**Mean**	**STD**
R	0.4604	0.0439	0.6135	0.0339
G	0.4141	0.0323	0.4940	0.0288
B	0.4632	0.0492	0.5066	0.0288

gorithm is so-called 'snake' [19, 29]. It is a general algorithm for matching a deformable model to an image by means of energy minimization. However, for this particular problem, the snake algorithm suffers from various local optimization problems associated with initialization, poor convergence to concave boundaries, vulnerability to image noise and has a high computational complexity. Since regular tongue shapes are known, it makes sense to apply a Deformable Template for segmentation [49, 34]. Deformable Template models have been successfully used in tracking objects, such as vehicles and human figures. It is found that they are more robust against noise and local shape distortions than snake algorithms. The tongue has a specific shape with "landmark points" lying within a certain variance of the trained set. The model allows deformation of the class of objects by learning patterns from the training set of correctly annotated images.

Models of more specific classes of shapes demand the use of some hard constraints and "default" shapes which are more interesting than a simple straight line. This can be achieved by using a parametric shape-model $\mathbf{s}(\mathbf{X})$, with relatively few degrees of freedom, known as a "deformable template". The template is matched to an image, in a manner similar to the snake, by searching for the value of the parameter vector $\mathbf{X}$ that minimizes the energy $E(\mathbf{X})$. The goal of the algorithm is to minimize the energy function: $E = E_{int} + E_{im} + E_{con}$, where, E_{int} is internal energy of the contour due to bending or discontinuities, E_{im} is energy due to image forces and E_{con} is energy due to external constraints.

In our study, we created a deformable template as shown in Fig. 2 and fit these templates to the image of the tongue by adjusting the various parameters that create the template of the tongue.

As shown in Fig. 2, we have the following parameters: x_o: center x-coordinate of the parabolic region. y_o: center y-coordinate of the parabolic region. α: angle (in radians) between the x-axis where the parabola ends and the line joining OO' equal to the length of the radius of the circle. r: radius of the circular portion (determined by a and α). θ: Angle (in radians) spanned by the circular arcs. Equation of parabola: $X = aY^2$, where a is a parameter that adjusts

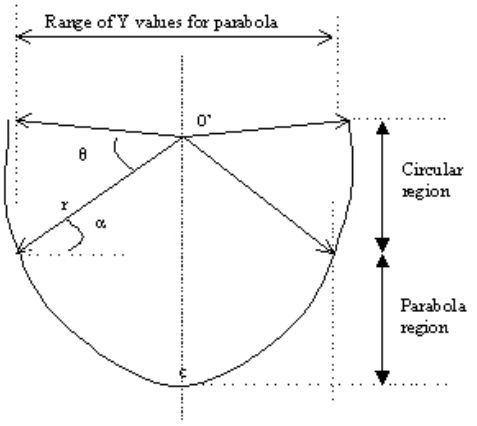

Fig. 2. Deformable Template.

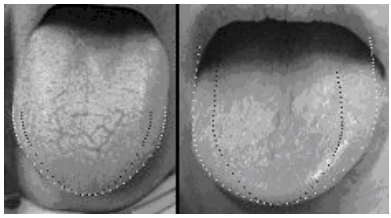

Fig. 3. Segmentation results (The black dots are the initial shape boundary and the white dots are the final shape boundary).

the thickness of the parabola. For the simplicity of the problem, we have not yet considered the axes rotation. Initially, we assumed symmetry in the tongue shape between the left and the right portions of the tongue. Then we accounted for more flexibility in the tongue shape by having different values of a, θ ($\theta_{1_{left}}$ and $\theta_{1_{right}}$), α ($\alpha_{1_{left}}$ and $\alpha_{1_{right}}$) and different parabola equations for the left and the right portions. Further, two additional circular portions were added to the left and the right portions giving different values for θ ($\theta_{2_{left}}$ and $\theta_{2_{right}}$), α ($\alpha_{2_{left}}$ and $\alpha_{2_{right}}$) and r. The template is given a good initial guess point (x_0, y_0). All the parameters are varied within a certain feasible limit (which defines the range of shapes the tongue template can take). The energy of the points (E) is calculated for all the possible templates. The average E is maximized and the resultant vector (or template corresponding to this maximum E) is the desired solution.

The algorithm was implemented in Matlab^{TM}. The black line indicates the initial starting template and the white line gives the final solution. Result samples are shown in Fig. 3.

Currently, we provide just a single point for the initial point (i.e. (x_0, y_0) or the lowest point of the tongue). It is desirable to provide more initial points that can be located visually. A total of 5 points on the tongue could fix the weakness mentioned above. Further, more constraints and finer step variations on the parameters can give more accurate results. Using an array of templates (instead of just a single template) can also give better results.

5 Feature Descriptions

Features on the tongue include color and texture. Most TCM practitioners do not have numerical descriptions of the color or texture features. Instead, they use analogies or qualitative descriptions, such as 'network-like cracks', or 'sandpaper-like surface'. It is possible to develop a scheme to map the qualitative descriptions to fuzzy sets of feature values.

However, in this chapter, we only discuss the numerical expressions of the features. In this study, we use CIE L*a*b* color space to represent the color features on the tongue. We also use several texture analysis methods that can correspond to human-descriptions of textures: 1) calculating fractal dimension

Db to represent roughness or smoothness of the tongue, 2) crack index CI to describe cracks on the tongue, 3) energy function for describing the roughness, and 4) entropy function to represent the order of the texture on the tongue:

$$\mathbf{F} = [\mathrm{a}^*, \mathrm{b}^*, \mathrm{Db}, \mathrm{CI}, \mathrm{energy}, \mathrm{entropy}] \tag{1}$$

5.1 Color Space Coordinates

The tongue project presents a unique challenge in the overall gross variance of the data set. There are tongues from different genders, ages and ethnic groups, which present unique difficulties in creating texture algorithms that are applicable to the entire data set. Minimal usage of parameters is key to developing a robust algorithm. A color space is a way of numerically describing a color. This almost always requires three numbers to accurately and succinctly describe all possible colors, as it is trivial to describe simple colors yet not so easy to describe colors like a faint red, in low-lighting. A simple example of a color space is that one may attempt to describe a color in terms of the actual color (red, orange, etc), its tint, or how deep the color is, and how much lighting there is on the color. Computer displays and televisions combine three primary colors (red, green and blue) in different proportions to form the different colors of the spectrum.

CIE 1976 L*a*b* is a color space that is an attempt to linearize the perceptibility of color differences. The non-linear relations for L*, a*, and b* are intended to mimic the logarithmic response of the eye, where L represents the lightness, a is the Redness/Greeness and b is the Yellowness/Blueness. However, the values from a digital camera are RBG-based. RGB values in a particular set of primaries can be transformed to and from CIE XYZ via a 3x3 matrix transform. To transform from RGB to XYZ (with D65 white point), the matrix transform used is [27, 39, 37]:

$$\begin{bmatrix} X \\ Y \\ Z \end{bmatrix} = \begin{bmatrix} 0.412453 & 0.357580 & 0.180423 \\ 0.212671 & 0.715160 & 0.072169 \\ 0.019334 & 0.119193 & 0.950227 \end{bmatrix} * \begin{bmatrix} R \\ G \\ B \end{bmatrix} \tag{2}$$

The L*, a*, and b* values can be converted from CIE XYZ, where coloring information is referred to the color of the white point of the system, subscript n. Here X_n, Y_n and Z_n are the tristimulus values of the reference white.

$$\mathrm{L}^* = \begin{cases} 116 * (\frac{Y}{Y_n})^{\frac{1}{3}} - 16 & \text{for } \frac{Y}{Y_n} > 0.008856 \\ 903.3 * \frac{Y}{Y_n} & \text{otherwise} \end{cases} \tag{3}$$

$$\mathrm{a}^* = 500 * (f\left[\frac{X}{X_n}\right] - f\left[\frac{Y}{Y_n}\right]) \tag{4}$$

$$\mathrm{b}^* = 200 * (f\left[\frac{Y}{Y_n}\right] - f\left[\frac{Z}{Z_n}\right]) \tag{5}$$

$$where\ f(t) = \begin{cases} t^{\frac{1}{3}} & \text{for } t > 0.008856 \\ 7.787 * t + \frac{16}{116} & \text{otherwise} \end{cases} \tag{6}$$

Since we tried to eliminate the lightness effect, we only used a* and b* as the color feature vector.

5.2 Fractal Dimensions

Fractal Dimension is another characterization of the texture on the tongue surface. Differential Box-Counting Dimension (DBCD) is an estimator of Hausdorff-Besicovitch dimension [8]. Like many other estimators of fractal dimension, DBCD is estimated by examining the relationship between a measure and the scale at which the measure was taken. DBCD is calculated on black and white images, where one value (for example, black) is taken to represent the object and the other value (white in this case) is taken to represent the background [28].

The image being measured was divided into equal sized squares. For a given size square (r x r pixels), the number of boxes containing any pixels belonging to the image, $N(r)$, is counted. This was done for several scales (several different r values), after which the relationship between $\log(N)$ and $\log(r)$ was calculated by finding the best-fit line between all r, $N(r)$ data points. The best-fit line corresponds to the relation:

$$N(r) = k \cdot r^{-Db} \tag{7}$$

The constant k is not important, but Db, the box dimension, is an estimator of fractal dimension. The implementation created for this project takes as a parameter an initial window size r to begin measuring. This window size was doubled repeatedly as long as the window size did not exceed the image size. Db was then calculated from the measurements taken at these scales. To adapt tongue images to be feasible for this algorithm, tongues were first converted to gray scale, using MatLab's `rgb2gray` function, and then from gray scale to black while running a Canny edge-detector on the gray scale image. The black and white image was analyzed using the DBCD algorithm described above.

5.3 Crack Detection

We also developed an algorithm to find and isolate cracks in the tongue. Cracks in the tongue can be an indicator of abnormality. Other crack detectors and classifiers [45, 46] have also been based on threshold and morphological operations in the primary stages. The system, outlined by Ukai [45], was used for detecting cracks in tunnel walls, and worked by using dynamic binarization (adaptive thresholding), dilation and erosion, eliminating particles, and analyzing the remaining particles. The interesting part of this system is its use of spatial frequency filters to distinguish between normal wall joints and cracks. It should be noted that this system appears to rely on hand-tuned parameters for each stage, which may be okay for its usage (provided that the equipment used to capture the input data, and the general properties of the walls do not change). A detector and classifier of cracks, described by Nieniewski et al [46], was used for analyzing cracked regions of ferrite. This system used morphological operations, bi-level thresholding, and a feature-based parallel K-nearest neighbor classifier [10]. This system was mainly intended for separating out cracks that are defects from grooves that occur from grinding. The morphological parts quickly generated all candidates for cracks, and the K-nearest neighbor classifier is used to

reject those candidates who matched a training set of grooves. This system is interesting for its use of a K-nearest neighbor classifier, however it also relied on the grooves in the material to normally lie in a uniform direction. Also, the initial portion of the detector depends on hand-tuned parameters for the morphological operation and thresholding operations.

Crack detection is a multiple stage process that attempts to find places where there are cracks in the tongue. Each stage is essentially a filtering process to attempt to get rid of more unwanted information. The essential steps behind of the process are:

1. *Find all pixels that are bright in the S channel and dark in the V channel.*
2. *Remove pixels that fall on the edge of the tongue, as the edge area often has the most extreme illumination variances and causes difficulties for accurately finding cracks.*
3. *Remove all particles in the image except the largest ones.*

To convert color coordinates from RGB to HSV (Hue, Saturation, and Value), we used the following pseudo code:

```
max = largest RGB component
min = smallest RGB component

     ⎧  60*(G-B)/(max-min)   if red is largest
H =  ⎨ 180*(B-R)/(max-min)   if green is largest
     ⎩ 300*(R-G)/(max-min)   if blue is largest

S = (max-min)/max
V = max
```

Step 1 is based on the discovery that cracks appear bright in the S channel, and dark in the V channel. HSV color space is another way of representing color image. Computers typically use the RGB color space, which separates color into its red, green and blue components. In the RGB color space, white is represented by red, green and blue being at maximum intensity. Purple is represented by putting red and blue at half-intensity, and green at zero intensity. HSV represents colors in a method more understandable by humans: H represents the hue, or actual color, S represents the saturation, which is essentially how strong the hue appears, and V is the overall illumination present.

The HSV color space is used to accentuate cracks. As stated before, cracks appear bright in the S channel and dark in the V channel. "Appearing" bright and dark, is relative to other pixels in the same channel, as they are actually darker in the S channel, and only appear brighter because they are relatively bright compared to their surrounding pixels. Therefore, the algorithm enhances this contrast by thresholding local blocks relative to themselves. This is different than a normal threshold that simply compares each pixel to a number such as the mean of the entire image. The problem with the normal approach is that near the edges of the tongue, there is a very high variation, which can throw

Fig. 4. Cracks on the Tongue.

off thresholding for the rest of the image. Since an adaptive threshold considers each block individually, this problem is avoided. For each window analyzed, the adaptive threshold sets its threshold first by finding the mean value and standard deviation of non-black pixels, and then setting a threshold based on these values. This allows the thresholder to provide consistent behavior for images with different illuminations, provided they fit a relatively normal lighting distribution, which was found to be typical for the tongues analyzed. For this project, the mean pixel value was used.

The next part of step one is to invert the V channel. This is done to reflect the fact that the cracks are dark in the V channel. By inverting it, the cracks (which would have been thresholded down to 0) are once again changed back to 1. The next step, essentially an "AND" operation on both images, chooses all pixels that appeared "bright" in the S channel and "dark" in the V channel.

At this stage, there is still a lot of noise. The main cracks, however, appear to be large, whereas the noise is limited down to small size pixels. To remove the noise in the image, the image is first eroded, then all remaining small pixels are removed. Eroding is a morphological operation that shrinks objects in an image, much like land erosion washes away dirt on hills, making the hills smaller. Erosion works by passing a structuring element over the image, and outputting a pixel only when the structuring element is completely covered by pixels in the original image [49].

Once the image has been eroded to enhance the separation of objects in the image, all objects belonging on the fringe edge of the image are removed. This is done to prevent erroneous detection of cracks that are really just places on the edge of the tongue where illumination falls off steeply. The first step in doing this is to calculate a mask that describes the edge of the tongue by thresholding the image. The mean pixel value of the non-black pixels in the image minus one-half of the standard deviation of the non-black pixel values is used as the threshold. Next, this mask is smoothed by performing a closing operation on it. Closing is simply dilating the image then eroding it, and has the effect of closing small gaps in the image. Just as dilating has its counterpart eroding, closing has a counterpart called opening which does the opposite by eroding then dilating.

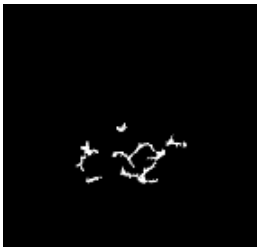

Fig. 5. Cracks detected by the algorithm.

The previous result image is then masked with the inverse of the tongue-edge mask to retain only data that does not appear on the edge of the tongue.

After all objects in the image are shrunken with erosion, the pixel groupings are separated out into particles so that they can be analyzed individually. This is done by scanning the image and grouping pixels that are connected to each other. There are two typical definitions of pixels being "connected" to another. According to the 4-way definition, a pixel is connected to a group if the group appears to the right, left, bottom or top of the pixel. Under the 8-way definition, a pixel is connected to a group if any of the bordering pixels are in the group.

Once all pixel groupings are determined, then only the largest pixel groupings are chosen. This is done simply by comparing the area of the group to a threshold value. The area of a group is the number of pixels that form it. The threshold value is calculated by taking the mean plus one standard deviation of particle area values. This is done to keep only "large" particles and exclude smaller particles that result from noise in the image. Figure 5 shows the finished crack-detected image.

In order to summarize the crack information of an image, we have developed a simple numerical descriptor to describe cracks called "Crack Index". Crack Index (CI), is a number between 0 and 100 that describes the content of cracks in the image.

$$CI = 100 * \frac{A_{cracks}}{A_{total}} \tag{8}$$

A CI of 0 indicates no cracks were found, whereas increasing values indicate an increasing density of cracks. Crack Index is calculated by taking the area of cracks divided by the area of the total tongue and multiplying by 100.

5.4 Describers for Texture Homogeneous and Complexity

To give further descriptions of texture details such as homogeneous and complexity, we use energy and entropy functions that are based on the co-occurrence matrix. It describes the repeated occurrence of some gray-level configuration in the texture [36]. P is a 2-D n x n co-occurrence matrix, where n is the number of gray-levels within an image. The matrix acts as an accumulator so that $P[i, j]$ counts the number of pixel pairs having the intensities i and j. The idea

is to scan the image and keep track of how often pixels that differ by Δz in value are separated by a particular distance d in position [49, 41]. Based on the co-occurrence matrix, we compute the energy function and entropy function for further texture descriptions. The energy function, or angular second moment, is an image homogeneity measure; the more homogeneous the image, the larger the value.

$$H_{entropy} = -\sum_{i,j} (P[i,j] \log_2(P[i,j])) \tag{9}$$

The entropy function, can also be used as a measure for "textureness or complexity."

$$H_{entropy} = -\sum_{i,j} \left(\frac{P[i,j]}{1+|i-j|} \right) \tag{10}$$

where, P is a gray level co-occurrence matrix that contains information about the position of pixels having similar gray level values.

6 Visualization Techniques and Process

In this section, we show how visualization can provide insights and facilitate the analysis and clustering of tongues based on feature values. We have a feature vector: F=[a*,b*,Db,CI,energy,entropy]. Li & Cai extracted the values for these six features for a set of 34 tongues which belong to people of five different diagnostic categories: Healthy (H), History of Cancers (HC), History of Polyps (HP), Polyps (P), Colon Cancer (C) [50]. We used this data set to demonstrate the visualization techniques and process.

6.1 Cluster Plots

The goal of data exploration is to investigate if there are some obvious correlations between different features. This can be achieved by 2D and 3D cluster plots. We found that there are definite patterns for some categories as summarized in Table 2. Figure 6 shows a 2D cluster plot of Db-entropy which shows a clear pattern for Healthy (H) and Polyps (P) cases.

As a* and b* are two chromatic dimensions in the L*a*b* color space, observed definite ranges of values for these features for certain diagnostic conditions indicate that there is a strong correlation between the tongue color and these diagnostic conditions. We also observe two outliers with very high crack index, one with a Healthy condition and one with History of Polyps and History of Cancer. This suggests that these are special cases where these tongues normally have lots of cracks, and the amount of cracks therefore does not reflect on the disease condition.

For 3D cluster plots, we used different colors and glyphs for each category (see Fig. 7) and allowed users to rotate them around each axis to facilitate viewing. Rotating the plots increased the sense of depth and the perception of clusters and correlations. We also observed that the high precision of the raw data might

Table 2. Observed patterns obtained from 2D and 3D cluster plots.

category	Db	CI	a*	b*	Energy	Entropy
HP	medium	low medium	narrow mid-range	mid-range	low	
P	high			mid-range	high	
HC	low	low	narrow mid-range	narrow mid-range		
C			low	very high		high
H	low Db	or high CI				

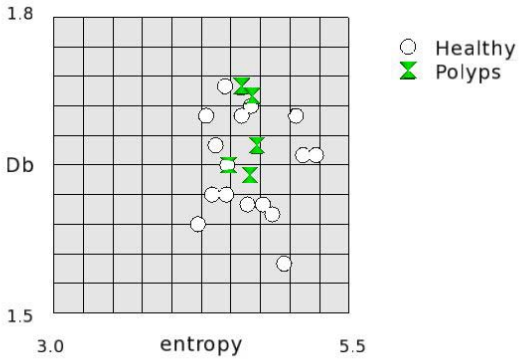

Fig. 6. 2D cluster plot of Db-CI.

have adverse effects on the cluster viewing (in other words, the precision was higher than what was required). We therefore tried different quantization scales and finally chose a 10-interval scale which was the coarsest scale that could still distinguish each data point. The plots for each triplet of features (with a* and b* being always kept together) re-confirm the observations summarized in Table 2.

We also wished to determine from the 3D cluster plots which triplets of features give better discriminating power, in order to use these as a starting point to gradually explore rules for clustering in higher dimensions using parallel coordinates. Figure 7 shows a 3D cluster plot (Db, a*, b*) for Healthy and Polyps cases. However, we observed that although there appeared to be some groupings, these groupings were not separable and the rules underlying these groupings were not simple. We investigated this problem further using another visualization method based on parallel coordinates, which allowed the simultaneous viewing of multi (more than 3) dimensions.

6.2 Discovery of Rules Using Parallel Coordinates Plots

High dimensional data is often transformed or projected to 2D or 3D representations for visualization. However, this practice usually causes a loss of information. Parallel coordinates allow n-dimensional data to be displayed in 2D [51]. In this method, n Cartesian coordinates are mapped into n parallel coordinates, and an

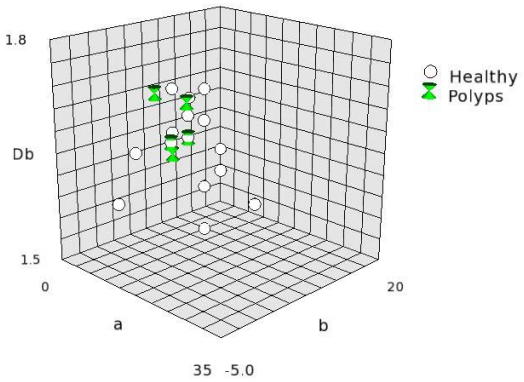

Fig. 7. 3D cluster plot for (Db,a*,b*) for H & P cases.

n-dimensional point becomes a series of $(n-1)$ lines connecting the values on n parallel axes. Berthold and Holve, [52] used this technique to visualize fuzzy rules underlying 3 classes of irises which resulted from a training set of 75 data samples with 4 features (petal length, petal width, sepal length, sepal width). Pham & Brown [54] extended this technique to 3D to provide better visualization of the membership function of the fuzzy sets and insight into the strength of the clustering. We now show how to apply these techniques to analyze the tongue data.

Since the set of data available at this stage only consisted of 34 tongues (6HP, 5P, 5HC, 2C, 16N), we attempted to cluster this data set through a display in six parallel coordinates: Db, CI, a*, b*, energy and entropy. Figure 8 shows the results for three categories: P, H and C. The shaded area representing each category is obtained by plotting the extent covered by the extreme values for each coordinate. It can be readily seen that these areas, though overlapped, are distinguishable from each other.

The order of the coordinates does not change the results, although it might affect the perceptibility. For example, a large number of intersections might cause confusion and make it difficult to discern the clusters. Thus, we provided tools to swap coordinates in order to choose the order with best perceptibility. We observed that the Cancer cases form a narrow band for all six coordinates as seen in Fig. 8.

We also observed that for Healthy cases, the variability in feature values is much greater than in the disease cases. However, this fact can only be confirmed when more data on disease cases is available. If a much larger set of data is available, it would also be possible to provide a more sophisticated visualization by integrating fuzzy sets and using 3D parallel coordinates. We discuss how this may be achieved in the next subsection.

6.3 Integration of Fuzzy Sets to Visualization

Fuzzy logic has been used extensively and successfully in many areas, especially in social sciences and engineering. While mathematical models are based on

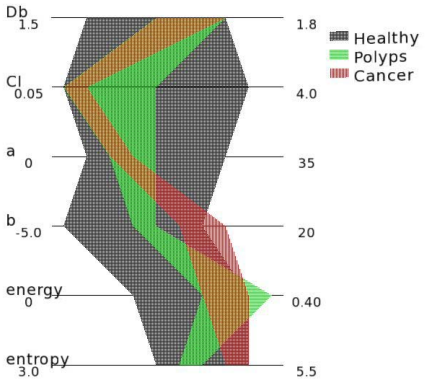

Fig. 8. Pattern of the cancer cases displayed in parallel coordinates.

algebraic operations (e.g. equations, integrals), logic models rely on logical connectives (and, or, if-then), often with linguistic parameters, which give rise to rule-based and knowledge-based systems. Fuzzy logic models can combine both of these types of modeling via the fuzzification of algebraic and logical operations. There are three common classes of fuzzy logic models: information processing model, which describes probabilistic relationships between sets of inputs and outputs; control models, which control the operations of systems governed by many fuzzy parameters; and decision models, which model human behavior incorporating subjective knowledge and needs, by using decision variables. For some applications, fuzzy systems often perform better than traditional systems because of their capability to deal with non-linearity and uncertainty. While traditional systems make precise decisions at every stage, fuzzy systems retain the information about uncertainty as long as possible and only draw a crisp decision at the last stage. Another advantage is that linguistic rules, when used in fuzzy systems, not only make tools more intuitive, but also provide better understanding and appreciation of the outcomes.

As more tongue data is available, it would be more appropriate to treat the extent of each feature value for each diagnostic category as a fuzzy set. The membership function for this fuzzy set can be computed from the frequency of each value. This membership value gives an indication of the confidence level that each value belongs to this set. Hence, the level of overall confidence that a given case belongs to a particular diagnostic category is the minimum of the membership values for all features. Since we have not yet obtained a large enough set of tongue data, we demonstrate this technique using the Iris data example. Figure 9 shows a 3D parallel coordinates display for this data set. The advantages of integrating fuzzy sets are two-fold. First, it provides an intuitive match with the way doctors fuzzily assess the condition of the tongues. Secondly, it is possible to select the tightness of clusters through the use of an alpha cut plane to discard those cases whose feature values have too low membership values (i.e. the level of confidence that a particular case belongs to a specific class is low).

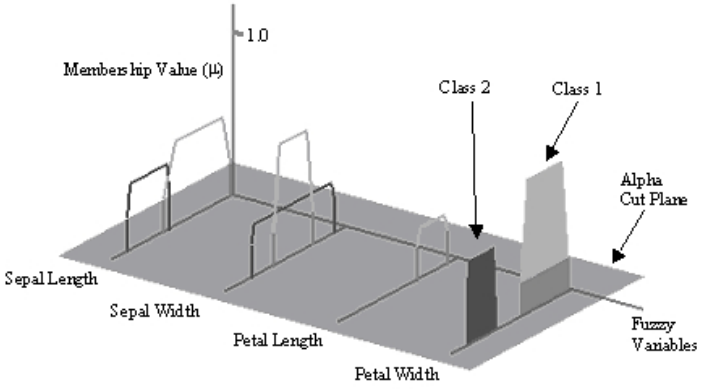

Fig. 9. A 3D parallel plot of Iris data example [Pham & Brown, 2003].

Another improvement can be made by asking doctors to provide the assessment of diagnostic categories with fuzzy grading. For example, instead of Healthy, three grades are introduced: Very Healthy, Moderately Healthy, and Slightly Healthy. Similarly, disease conditions can be expressed in three grades: Very Serious, Moderately Serious, Slightly Serious. Such fuzzy assessment would match more faithfully with real diagnosis practice. By linking fuzzy values for the color and texture features of the tongue with fuzzy diagnostic categories, it is envisaged that a more accurate classification of cases would result. However, in order to achieve this, we will need to collect more cases and more detailed diagnosis from doctors for each case.

7 Diagnosis with Neural Computing

Fuzzy visualization methods provide a promising interface for medical doctors to interact with the ambient diagnostic systems, especially at the early explorative stages. As we gain more insight about the data, it is time to build numerical models for diagnosis.

Ambient diagnostics is made largely by the interconnected elements. The metaphor can be simulated by artificial neural networks, which are composed of simple elements operating in parallel. We can train a neural network to perform a particular diagnostic function by adjusting the values of the connections (soup of weights) between elements. In the supervised learning process, many such input/target pairs are used to train a network [62].

Radial Basis Network is a feedforward backpropagation network. It is fast but needs more neurons so requires more memory [63]. It is also simple to be implemented on hardware, for example, a neural network on a chip, can perform 1 million recognitions per second. In a radial basis function network, each hidden unit produces a ball-shape 'pulse' driven by a Gaussian function. The output unit produces a linear combination of hidden unit pulses. In this case,

$$R(n) = e^{-n^2} \tag{11}$$

Table 3. Test samples (not included in the training dataset).

data set	target	Db	CI	a*	b*	energy	entropy
1	10 (P)	1.68	0.62	18.76	9.97	0.25	4.76
2	10 (P)	1.73	1.92	7.75	4.73	0.33	4.59
3	5 (HP)	1.64	0.55	9.98	5.35	0.33	4.66
4	5 (HP)	1.64	1.23	13.07	5.84	0.19	5.12
5	1 (NP/NHP)	1.63	0.1	11.55	8.77	0.33	4.91
6	1 (NP/NHP)	1.61	0.61	24.56	6.08	0.16	4.64

Table 4. Results for three types (spread factor = 0.4).

data set	target	GRNN	PNN
1	10 (P)	5 (HP)	5 (HP)
2	10 (P)	1 (NP/NHP)	1 (NP/NHP)
3	5 (HP)	4.56 (HP)	5 (HP)
4	5 (HP)	2.46 (NP/NHP)	1 (NP/NHP)
5	1 (NP/NHP)	1 (NP/NHP)	1 (NP/NHP)
6	1 (NP/NHP)	1 (NP/NHP)	1 (NP/NHP)

We test two variations of radial basis function: probabilistic neural network (PNN) and generalized regression neural networks (GRNN) provided by Mathworks [62]. Probabilistic neural networks (PNN) are suitable for classification problems. The PNN model $f(P, T, spread)$ takes three arguments: P is an R x Q matrix of Q input vectors; T is an S x Q matrix of Q target class vectors; and *spread* is the width of the radial basis function. To fit data very closely, we use a spread smaller than the typical distance between vectors. To fit the data more smoothly, we have to use a larger spread value. Generalized regression neural networks (GRNN) [61] are a radial basis network that is often used for function approximation. The GRNN model $f(P, T, spread)$ takes three inputs: P is an R x Q matrix of Q input vectors; T is an S x Q matrix of Q target class vectors; *spread* again is the width of the bottom of the radial basis function.

We used 28 samples to train the neural networks and another 6 samples to test the models. In our first case, we considered three types of targets: Polyps (P=10), History of Polyps (HP = 5), and the rest of the cases (NP/NHP = C = HC = H = 1). The test data set is listed in Table 3. We have the results in Table 4.

In the second test case, we only considered two types of targets: either Polyps (P = 10), or Non-Polyps (NP = 1). The input data set is listed in Table 5 and the results are in Table 6.

As the two test scenarios show, PNN performs the same as GRNN. Also we learned that neural networks work better when the target classes are fewer, e.g. in our cases, two targets are better than three targets. Although both GRNN and PNN can correctly identify 2 out of 3 Polyps cases, it just may be a result of the over-simplified process. It is not necessary to imply that these methods

Table 5. Test samples (not included in the training dataset).

data set	target	Db	CI	a*	b*	energy	entropy
1	10 (P)	1.68	0.62	18.76	9.97	0.25	4.76
2	10 (P)	1.64	0.55	9.98	5.35	0.33	4.66
3	10 (P)	1.73	1.92	7.75	4.73	0.33	4.59
4	1 (NP)	1.63	0.1	11.55	8.77	0.33	4.91
5	1 (NP)	1.61	0.61	24.56	6.08	0.16	4.64
6	1 (NP)	1.72	1.17	11.53	11.34	0.26	4.46

Table 6. Results for two types (spread factor = 0.4).

data set	target	GRNN	PNN
1	10 (P)	10 (P)	10 (P)
2	10 (P)	9.0049 (P)	10 (P)
3	10 (P)	1 (NP)	1 (NP)
4	1 (NP)	1 (NP)	1 (NP)
5	1 (NP)	1 (NP)	1 (NP)
6	1 (NP)	1 (NP)	1 (NP)

would work well with a larger sample size. There is still a long way to go before we can come up with a selective and robust classification method for the tongue inspection.

8 Conclusions

Ambient Diagnostics is a contemporary technology that is inspired by ancient medical practices. The goal is to detect abnormities from seemly disconnected ambient data. In this chapter, we focused on computerized tongue inspection. Our research started with collecting tongue samples at a clinical lab setting and building conceptual prototypes for scientific discovery along the way. The explorations include digital imaging, color calibration, feature descriptions, visualization and neural computing. From this preliminary study, we have learned the following lessons:

The portable tongue scanner is more reliable than the digital camera in terms of invariance of illumination, reflection and angles. However, its resolution is low and cost is rather high. We will do further investigation to reduce the cost and increase the resolution.

Previous TCM studies have shown strong correlations between the color of tongue coating and cancers. We found that the texture characteristics on the tongue surface is more sensitive to the colon polyps (pre-cancerous) or history of polyps than color characteristics. This discovery will lead us in a new direction toward effective tongue feature expressions, such as adding more texture describers in the feature vector. The more dimensions of the describers, the more accurate the classification and recognition of the model. We had four dimensions:

Energy, Entropy, Crack Index, and Fractal Dimension. We plan to add six more in the near future. In addition, we will add TCM expert's verbal descriptions into the model. We need to devise a scheme to map these qualitative descriptions into fuzzy sets of quantitative values so that computers can process them.

As comparing one patient's tongue to another patient's tongue is difficult in terms of shape, color and texture registration, we found that it is more accurate to compare the tongue images at a personal basis, e.g. the images of a cancer patient before and after chemo, etc. It could be used as a measurement of the effectiveness of a treatment. This is similar to the self-monitoring process that has been used in the head injury study with fMRI personal data. For each person, we can establish a base line and then use ubiquitous computing technologies to monitor the patient and compare the collected data to the base line at a predefined duration.

Neural computing is a promising method for generating diagnostic results and potentially can be hardened onto a chip that is less than one dollar. We use two neural networks for testing the concept: a general regression neural network (GRNN) and a probabilitistic neural network (PNN). As the two test scenarios show, both have virtually the same performance. Also we learned that neural networks work better when the target classes are fewer, e.g. in our cases, two targets are better than three targets. Although PNN and GRNN can correctly classify 2 Polyps test cases out of 3, it should not be implied that the methods would work well with a larger sample size. We still need more work to verify the selectivity and reliability of the models.

Visualization utilities are helpful in early stage data explorations. At this stage, the aim of visualization is to provide tools to aid the analysis, rather than to provide a precise proof of clustering decisions that can be provided by statistical and data mining techniques. We have not yet coupled visualization techniques with fuzzy algorithms. The 3D clustering figures were actually an animation that allows viewing from different angles with different triplets of variables. Clusters are observed in some cases, while in other cases, we could not see clusters. It is also not possible to see this effect when viewed as a figure on a flat piece of paper. The parallel coordinates approach provides multi-dimensional visualization. Although the variable values may overlap, as clusters, they do have distinct characteristics.

As more tongue data is available, we will be able to use more advanced techniques for visualization and classification of tongues to obtain better analysis and more accurate classification. We have received letters from a few colon cancer patients who have had 'geographical tongues'. Those feedbacks are significant resources for investigation. The combination of the tongue feature changes and other medical indications will increase the effectiveness of early diagnosis. We will continue to follow up the cases.

Affordable self-diagnostic kits are changing our lives. Decades ago, diabetes patients had to check their blood glucose in a lab or burn the sample with a candle. Today, they can buy a digital kit from a drugstore and test anywhere. Modern electronic technologies have been the building blocks for eDiagnostic

kits. According to Gorden E. Moore's famous paper in 1965 [64], transistor density on integrated circuits doubles every couple of years. This exponential growth and ever-shrinking chip size results in more affordable Ambient Diagnostic devices.

Errors or mistakes are as inherent a possibility for ambient intelligence in scientific discovery as they are to any human activity. This initial study is no exception. Nevertheless, we hope that by presenting our findings we may inspire further explorations in this area of research.

Acknowledgements

We are deeply indebted to all of our supporters of this study, including the sponsor, Senior Project Officer Ms. Nancy Zionts from the Jewish Health Foundation. We are grateful for the clinical investigation and the IRB Process from Dr. Ron Herberman, Dr. Robert Schoen, Ms. Karen Foley and Ms. Betsy Hela from the University of Pittsburgh Medical Center, Pittsburgh Cancer Institute. The results and conclusions expressed by the authors in this chapter do not necessarily state or reflect those of their sponsors and supporters.

References

1. Spiteri, M.A., Cook, D.G., Clarke, S.W.: "Reliabilty of eliciting physical signs in examination of the chest." Lancet. 2:873-75. (1988)
2. Pasterkamp, H., Kraman, S.,S., Wodicka, G.R.: "Respiratory sounds: advances beyond the stethoscope." American Journal of Respiratory Critical Care Medicine. 156:974-87 (1997)
3. Anderson, K., Qiu, Y., Whittaker, A.R., Lucas, Margaret: "Breath sounds, asthma, and the mobile phone." Lancet. 358:1343-44. (2001)
4. Kaiser, R.: "Smart toilet a sure sign of future technology." Chicago Tribune. Saturday December 23. (2000)
5. Bodymedia: www.bodymedia.com
6. Givenimaging: www.givenimaging.com
7. McDermott, M.M. et al: "Functional Decline in Peripheral Arterial Disease: Associations With the Ankle Brachial Index and Leg Symptoms." JAMA, July. 292:453-461 (2004)
8. Yu, H., MacGregor, J., Haarsma, G., and Bourg, W.: "Digital Imaging for Online Monitoring and Control of Industrial Snack Food Processes." Ind. Eng. Chem. Res. 42. (2003) 3036-3044
9. Cai, Y.: "Trajectory Mapping for Landmine Detection." Lecture Notes in Computer Science, Edited by Peter M.A. Sloot et al, LNCS 2657, Computational Science, ICCS 2003, Part III, Springer-Verlag. (2003)
10. Hornbeckz, R. W.: Numerical Methods. Printice-Hall, Inc., Englewood Cliffs, New Jerscy. (1995)
11. Wu, H., Siegel, M., Stiefelhagen, R., and Yang, J.: "Sensor Fusion Using Dempster-Shafer Theory." The Proceedings of IMTC 2002. Anchorage, AK, USA, May 21-23. (2002)

12. Wu, H., Siegel,M. and Khosla,P.: "Vehicle Sound Signature Recognition by Frequency Principle Component Analysis." The Proceedings of IMTC 1998 , selected in the IEEE Transaction on Instrumentation and Measurement Vol. 48, No. 5, ISSN 0018-9456. October. (1999) 1005-1009
13. Feigenbaum, E.A. and Simon, H.A.: "EPAM-Like model of recognition and learning." Cognition Science. 8:305-360 (1984)
14. Zadeh, L.: "Fuzzy Sets." Journal of Information and Control, Vol.8. (1965) 338-353
15. Cai,Y., Hu, Y., Siegel, M., Gollapalli, S., Venugopal, A., Bardak, U.: "Onboard Feature Indexing from Satellite Lidar Images." IEEE IWADC, Perugia, Italy. (2003)
16. Post, Frits H., Nielson, Gregory M., Bonneau, Georges-Pierre (Eds.): Data Visualization: The State of the Art Series: The Kluwer International Series in Engineering and Computer Science. Vol. 713. (2002) http://www.springeronline.com/sgw/cda/frontpage/0,11855,5-149-69-33109107-0,00.html
17. Schroeder, W., Martin, K. and Lorensen, B.: The Visualization Toolkit. 2nd Edition, Prentice Hall, PTR. (1998)
18. Hraralick, R.M., Shanmugam, K., and Dinstein, I.: "Texture features for image classifaction." IEEE Transactions Systems, Man and Cybernetice, 3:610-621. (1973)
19. Cai, Y.: "A novel imaging system for tongue inspection." IEEE Instrumentation and Measurement Technology Conference, AK, USA, May. (2002)
20. Yao, P.: Comparison of TCM Tongue Images with Gastroscopy Images. Shangdong S&T Publisher, ISBN 7-5331-1849-9. in Chinese. (1996)
21. Li,N.M.: "130 cases of tongue analysis for liver patients." Journal of TCM & Western Medicine, Vol.6, No.3. in Chinese. (1986)
22. Chang,R. and Chen, R.S.: "Clinical studies for tongues of lung cancer patients." Journal of New TCM, No.7. in Chinese. (1987)
23. China Cancer Society & TCM Group.: "12448 clinical case studies of cancer patients' tongue images." Lung Cancer, Vol.7, No.3. in Chinese. (1987)
24. Chen, Z.L., et al.: "1046 case studies of cancer patients' tongues." Journal of TCM & Western Medicine, Vol.1, No.2. in Chinese. (1981)
25. Fang, D.R., Li,R.F., Li,X. and Fang, G.X.: "Stomach cancer patients' tongue images and analysis." Journal of TCM, No.10. in Chinese. (1991)
26. Zhang, E.: Diagnostics of Traditional Chinese Medicine. Publishing House of Shanghai University of Traditional Chinese Medicine, ISBN 7-81010-125-0. in both Chinese and English. (1990)
27. McCamy,C.S. et al: "A Color Rendition Chart." Journal of Applied Photographic Engineering, Summer Issue 1976, Vol.2, No.3. (1976) 95-99
28. Parker, J.R.: Algorithms for Image Processing and Computer Vision. Wiley Computer Publishing. (1976)
29. Akgul, Y.S., et at.: "Automatic Extraction and Tracking of the Tongue Contours." IEEE Trans. on Medical Imaging. Vol.18, No.10, October. (1999)
30. Watsuji, T., Arita,S., Shinohara,S., Kitade,T.: "Medical Application of Fuzzy Theory to the Diagnostic System of Tongue Inspection in Traditional Chinese Medicine." IEEE International Fuzzy Systems Conference Proceedings. (1999) 145-148
31. Jang,J.H., Kim,J.E., Park,K.M., Park,S.O., Chang,Y.S., Kim,B.Y.: "Development of the Digital Tongue Inspection System with Image Analysis." Proceedings of the Second Joint EMBS/BMES Conference. Houston, TX, USA. October 23-26. (2002)

32. Vico,P.G., Dequanter,D., Somerhausen,N., Andry,G., Cartilier,L.H.: "Fractal Dimension of the Deep Margin of Tongue Carcinoma: A Prognostic Tool." Microscopy and Analysis (The Americas). (2003) 19-21
33. Pang,B., Zhang,D.: Tongue Image Analysis for Appendicitis Diagnosis. (2002)
34. Xu,L., et al.: "Segmentation of skin cancer images." Image and Vision Computing 17. (1999) 65-74
35. Esgiar,A.N., Sharif,B.S., Naguib,R.N.G., Bennett,M.K., Murray,A.: "Texture Descriptions and Classification for Pathological Analysis of Cancerous Colonic Mucosa." IEEE Conference on Image Processing and Its Applications, No. 465. (1999) 335-338
36. Haralick, R.M.: "Statistical and structural approaches to texture." Proceedings of the IEEE, vol. 67, no. 5. (1979) 786-804
37. Amots, H.: "Machine vision monitoring of plant nutrition." Ph.D. Dissertation, Purdue University. (1994)
38. Backhaus,W.G.,Kliegl,R.,Werner,J.S.: Color vision. Walter de Gruyter. (1998)
39. McLaren, K.: "The development of the CIE 1976 (L*a*b*) uniform colour-space and colour-difference formula." Journal of the Society of Dyers and Colourists 92. (1976) 338-341
40. Agoston, G. A.: "Color Theory and Its Application in Art and Design." Heidelberg. (1979)
41. Gotleib, L.C., and Kreyszig, H.E.: "Texture descriptions based on co-occurrence matrices." Computer Vision, Graphics and Image Processing, vol. 51, no. 1. (1990) 70-86
42. Gose, E., Johnsonbaugh, R., and Jost, S.: Pattern Recognition and Image Analysis. Prentice-Hall PTR, Englewood Cliffs, NJ. (1996) 372-379
43. Kaplan,L.M.: "Extended Fractal Analysis for Texture Classification and Segmentation." IEEE Transactions on Image Processing, Vol. 8, No. 11. (1999) 1572-1584
44. Ait-Kheddache, A.: Classification of Textures Using Higher-Order Fractal Dimensions. NCSU Department of Electrical and Computer Engineering. (1998)
45. Ukai,M.: Developing an Image Processing Algorithm for Detection of Deformations of Tunnel Walls. http://www.rtri.or.jp/infoce/qr/1997/v38_3/news2.html
46. Nieniewski,M., Chmielewski,L., Jozwik,A., Sklodowski,M: "Morphological Detection and Feature-Based Classification of Cracked Regions in Ferrites." Proc. of IPMAM '99, Warsaw. (1999)
47. Reed, T. R., and DuBuff, J.M.H.: "A review of recent texture segmentation and feature extraction techniques." CVGIP: Image Understanding, vol. 57, no. 3. (1993) 359-372
48. Tamura, H., Mori, S., and Yamawaki, T.: "Texture features corresponding to visual perception." IEEE Transactions, SMC, vol. 8. (1978) 460-473
49. Sonka, M, et al.: Image Processing, Analysis and Machine Vision. PWS Publishing. (1999)
50. Li,G. and Cai, Y.: "Texture analysis for tongue analysis." Technical Report BV-2003-2, School of Computer Science, Carnegie Mellon University. May. (2003)
51. Inselberg, A and Dimsdale, B.: "Multidimensional lines i: representation." SIAM J. Applied Math, 54(2). (1994) 559-577
52. Hall, L. and Berthold, M.: "Fuzzy Parallel Coordinates." Fuzzy Information Processing Society, NAFIPS. 19th International Conference of the North American, Atlanta, GA, USA. (2000) 74-78
53. Mitchell, T.: Machine Learning. McGraw Hill. (1997)

54. Pham, B. and Brown, R.: "Multi-agent approach for visualisation of fuzzy systems." ICCS '03 International Conference on Computational Science, Melbourne, June. (2003) 995-1004
55. Bezdek, J.C.: Pattern Recognition with Fuzzy Objective Function Algorithms. Plenum Press, New York. (1981)
56. Kohonen, T.: Self-organization and Associative Memory. 2nd edition, Springer, Berlin. (1988)
57. Picton, P.: Neural Networks. 2nd edition, Palgrave, Basingstoke. (2000)
58. Spath, H.: Cluster analysis algorithms. Ellis Horwood Ltd., Chichester. (1980)
59. http://www.gretagmacbeth.com/
60. Chaney, G.R. Do you Snore?
http://www.garnetchaney.com/help_*for*_snoring.shtml
61. Wasserman, P.D.: Advanced methods in neural computing. New York, Nostrand Reinhold. (1993)
62. Mathworks. Manual of the Neural Network Toolbox, MATHWORKS. (2004)
63. Chen, S., Cowan, C.F.N., and Grant, P.M.: "Orthogonal least squares learning algorithm for radial basis function networks." IEEE Transactions on Neural Networks, Vol.2, no.2, March. (1991) 302-309
64. Moore, G.: "Cramming more components onto integrated circuits." Electronics, Vol. 38, No. 8, April 19. (1965)
65. Gunarathne, G.P. Presmasiri, Gunarathne, Tharaka R.: "Arterial Blood-Volume Pulse Analyser." IEEE, Instrumentation and Measurement Technology Conference, AK, USA, May. (2002) 1249-1254